Indian Journal of Chemistry
Vol. 60A, March 2021, pp. 386-396

Ethanol condensation to butanol and higher alcohols over nickel and cobalt decorated CeO_2-Al_2O_3 mixed oxide catalysts

R Vinayagamoorthi[a,b], K R Krishnamurthy[b], B Viswanathan[b] & K Shanthi[a,*]

[a]Department of Chemistry, Anna University, Chennai 600 025, Tamil Nadu, India

[b]National Center for Catalysis Research, Indian Institute of Technology Madras, Chennai 600 036, Tamil Nadu, India

*E-mail: shanthiramesh@annauniv.edu

Received 13 June 2020; revised and accepted 08 December 2020

A new series of bimetallic Ni-Co catalysts, prepared by step wise substitution of Ni by Co, in mono metallic Ni (8%)/ CeO_2 -Al_2O_3, with the compositions of 6%Ni-2% Co, 4%Ni-4%Co, 2.5%Ni-5.5%Co and 8%Co, have been evaluated for conversion of ethanol to butanol and higher alcohols according to Guerbet alcohol chemistry. XRD, TPR and XPS studies reveal the formation of Ni-Co alloys at specific bimetallic compositions. Maximum reducibility is observed for the composition 4%Ni-4%Co, which also displays maximum ethanol conversion (55.1%) with C_{4+} alcohols selectivity of 50.2%, which are higher than those realized for mono metallic Ni and Co catalysts. Ni-Co alloys in bimetallic catalysts promote the crucial ethanol dehydrogenation and C_4 and C_{4+} aldehydes hydrogenation steps in the Guerbet process, thereby increasing ethanol conversion and C_{4+} alcohol selectivity. Selection of bimetallic catalysts with optimum compositions seems to be one of strategies to improve ethanol conversion and selectivity for higher alcohols.

Keywords: Ethanol condensation, Guerbet alcohols, Co-Ni bimetallic catalysts, hydrogenation, Ceria-alumina

Bioethanol, classified as carbon neutral fuel[1], is produced on large scale by the fermentation of different biomass feed-stocks[2]. Global production of bioethanol, estimated at 27050 Million gallons in 2017[3], is expected to grow at a CAGR of 5.3% during 2018-2024. Besides its use as bio-fuel, highly useful and value-added chemicals, like, acetic acid, ethyl acetate, ethylene, hydrogen, isobutene, acetaldehyde, 1,3-butadiene and butanol could be produced from abundantly available bioethanol[4]. Especially, the process for the conversion of ethanol to butanol has received global attention, since butanol has superior fuel characteristics compared to ethanol, and is widely accepted as the future biofuel. The process is based on the classical Guerbet chemistry[5] that involves condensation of a primary or secondary alcohol, either with itself or another alcohol, to yield higher carbon number alcohol. Various types of heterogeneous[6] as well as homogeneous catalysts[7] have been reported for the synthesis of Guerbet alcohols. Catalysts based on solid bases, basic zeolites, hydroxyapetite, hydrotalcite and alumina and carbon supported metal catalysts have been explored extensively[6-8]. Dehydrogenation of ethanol to acetaldehyde, followed by aldol condensation of acetaldehyde to crotonaldehdye and subsequently its hydrogenation of crotonaldehdye to butanol are the key reaction steps involved in the Guerbet process. Accordingly, dehydrogenation, hydrogenation, acidity and basicity are the requisite functionalities for the catalysts. Alumina supported metal (Co, Ni, Cu) catalysts possess unique combination of these functionalities and hence have been studied in detail[9-23]. While the metal (Co, Ni, Cu, Ru, Pd, Rh) function facilitates dehydrogenation and hydrogenation steps, inherent basicity and acidity in the alumina phase catalyze the aldol condensation and subsequent dehydration reaction, to yield C_4 and C_{4+} aldehydes, the crucial intermediates in the formation of butanol and higher alcohols. In this respect, alumina as a versatile support is amenable for tuning the acidity-basicity and the metal function by addition of suitable promoter oxides. Detailed studies on nickel catalysts supported on modified (with lanthana, ceria, zirconia, magnesia and titania) alumina support has been reported earlier[24].

Investigations by Riittonen et al.[11a,11b] on various alumina supported metal catalysts have revealed that Ni, Co and Cu based catalysts display superior performance compared to other metal (Ru, Pd, Rh, Ag and Au) based catalysts. Earlier studies by Yang et al.[10] on comparative evaluation of Fe, Co and

Ni supported on alumina catalysts, have shown that Fe displayed very low ethanol conversion (2%) while Co and Ni, moderate and nearly same activity (17-19%). While the selectivity for butanol was significantly high at 64.3% with Ni, it was considerably less with Co, at 22.7%, due to the formation of side products/intermediates, like, ethyl acetate (29.2%) butyraldehyde (15.9%) and acetaldehyde (14.1%). The product patterns thus indicate that, while both Ni & Co are almost equally active for ethanol dehydrogenation, aldol condensation of acetaldehyde and hydrogenation of butyraldehyde are relatively slower with Co. Among alumina supported Cu, Ni and Co catalysts, Ni/Al_2O_3 displays high activity and selectivity for butanol, while with Co/Al_2O_3, formation of ethyl acetate is favoured and is attributed to the presence of Co^{2+} ions in tetrahedral environment[11b]. Selectivity on Cu/Al_2O_3 is reported to be dependent on loading of Cu. Lower loading of Cu resulted in higher selectivity for butanol and higher loading leads to the formation of ethyl acetate[11b]. It is proposed that for the dehydrogenation of different alcohols, the use of transition metals in the reduced form (Co, Ni, Cu, Fe, Ir, etc.) reduce the activation energy of the α-CH bond scission. In addition, reduced metals could also alter the acid/base sites distribution.

Another approach by Zhang et al.[25] using commercial cobalt (Co) metal powder as a recyclable catalyst yielded butanol selectivity of 69% and yield of 2.89 mol %, but the process required long reaction time of 3 days. Besides the active metals like Ni, Co and Cu, the support characteristics play crucial role in controlling activity and selectivity for ethanol conversion. Quesada et al observed that Mg-Al mixed oxides function as active and stable supports for ethanol conversion[26] and with Co, Ni[27] and Ru[28,29] as active metals, displays substantial increase in selectivity towards butanol. Wu et al.[30] reported a series of activated carbon (AC) supported $M\text{-}CeO_2$ catalysts (M= Cu, Co, Ni, Pd and Fe) for catalytic upgrading ethanol to n-butanol highlighting inherent capabilities of metals for dehydrogenation and hydrogenation. Co, Ni and $Pd\text{-}CeO_2/AC$ catalysts exhibit higher selectivity towards n-butanol (47.6, 50.6 and 67.6%, respectively), but lower ethanol conversions. It was proposed that since the selectivity to n-butanol mainly depends on the formation and hydrogenation of crotonaldehyde steps, the trend in selectivity to n-butanol (Fe < Cu < Co < Ni < Pd) should be ascribed to the difference in the capability of hydrogen activation over active metals, as well as the aldol condensation of acetaldehyde over basic sites. However, ethanol conversion displays the opposite trend (Cu > Co > Ni > Fe > Pd) since dehydrogenation and hydrogenation is a pair of reverse catalytic processes[29].

It is clear that the selection of suitable metal and support functions are crucial for ethanol conversion and selectivity to higher alcohols. Only a few reports on the application of bimetallic catalysts, namely, Au-Ni and Au-M, with M=Fe, Co, Ag and Zr (16) and Cu-Ni and Cu-Ni-Mn[13,31,]for ethanol conversion have been published so far. In the present work, we have attempted to study the importance of bimetallic Ni-Co catalysts with varying Ni and Co contents, supported on ceria modified alumina. Considering their crucial role in dehydrogenation and hydrogenation functions, catalysts with different Ni and Co contents have been investigated to bring out possible synergistic effects between the two metals.

Materials and Methods

Chemicals

Pseudo boehmite (AlOOH) (Pural SB, Sasol, Germany), Nickel acetate [$Ni(CH_3COO)_2.4H_2O$], Cobalt acetate [$Co(CH_3COO)_2.4H_2O$[, Cerium nitrate hexahydrate [$(Ce(NO_3)_2.6H_2O$) (99.9%, CDH)], were used as received. Absolute alcohol (99.9%) from Changshu Hongsheng Fine Chemical Co. Ltd., China, was used for carrying out reactions.

Preparation of support and catalysts

Gamma alumina ($\gamma\text{-}Al_2O_3$) was prepared by calcination of pseudo boehmite (AlOOH) at 450 °C for 4 h. Al_2O_3 was impregnated separately with required quantity of cerium nitrate $Ce(NO_3)_3.6H_2O$, (to obtain 5% w/w of ceria in alumina) dissolved homogeneously in 20 mL of distilled water. After evaporation of excess water, the slurry was dried in air at 120 °C for 12 h and then calcined at 600 °C for 12 h in N_2 atmosphere. Ni (2.5% to 8% w/w) and Co (2% to 8% w/w) as nickel acetate and cobalt acetate respectively, were loaded on modified alumina by wet impregnation, dried at 120 °C for 12 h, followed by reduction in H_2 flow at 500 °C for 12 h.

Characterization of catalysts

Powder X-ray diffraction (XRD) patterns for the catalysts were recorded using Rigaku Corporation, Japan, Model Miniflex IIX-ray diffractometer, with Cu-Kα (λ =0.15418 nm) radiation in the 2θ range of

10° to 80° and at a scan rate of 3 °C/min. Crystallite size of the catalyst was calculated by X-ray line broadening analysis, using Debye-Scherrer equation.

N_2 adsorption and desorption isotherms were measured at 77 K using a Micromeritics ASAP 2020 unit. Surface area of the catalysts were measured by BET method and pore volume and pore size distribution by BJH method. Temperature programmed reduction (TPR) and temperature programmed desorption (TPD) of ammonia and carbon dioxide were performed on TPR/TPD ChemBET Chemisorption Analyzer (Quanta Chrome Instruments, USA) equipped with a thermal conductivity detector (TCD). For TPR measurements, the catalysts were calcined in air at 300 °C, prior to TPR experiments. 50 mg of calcined catalyst was pre-treated at 300 °C in high purity Ar gas (25 cc/min) for 1 h and then cooled to room temperature in Ar flow. The gas was changed to 10% H_2 in Ar (25 cc/min) at room temperature. After the stabilization of the baseline, TPR patterns were recorded from room temperature to 800 °C with a heating rate 10 °C/ min.

For TPD of ammonia, 50 mg of the reduced catalyst was pre-treated at 300 °C in helium flow of 20 mL/min for 1 h and cooled to room temperature in helium flow. The sample was saturated with ammonia by passing 10% NH_3 in helium gas over the catalyst for 20 min. After flushing out weakly adsorbed ammonia with helium flow at 373 K, the base line was established. TPD of adsorbed ammonia was then recorded by heating the sample in helium flow upto 650 °C with a heating rate of 10 °C per min. For TPD of CO_2 similar procedure was adopted using CO_2 as probe molecule instead of ammonia.

X-ray photoelectron spectra (XPS) of the reduced catalysts were recorded using Omicron Nanotechnology, Oxford Instruments, UK, instrument with Mg K_α radiation. The base pressure of the analysis chamber during the scan was 2×10^{-10} millibar. The pass energies for individual scan and survey scan are 20 and 100 eV, respectively. The spectra were recorded with step width of 0.05 eV. The data were processed with the Casa XPS software. Diffuse reflectance spectra (DRS) of the catalysts were recorded using JASCO Model V-650 UV-visible spectrophotometer.

Evaluation of catalysts for ethanol conversion

Reactions were carried in batch mode, using 100 mL Parr reactor with Model 4848 controller unit (Parr instruments, Chicago, USA). 1.83 g of catalyst was dispersed in 20 g of ethanol. After purging three times with N_2 to remove air, the reactor was filled with nitrogen up to 10 kg/cm^2 and sealed. The reaction was carried out under autogenous pressure at 200 °C for 8 h with an agitator speed of 350 rpm. During the reaction, the reactor pressure increased gradually with time and stabilized at 45-50 kg/cm^2 after 4 h. After the completion of 8 h, the reactor was cooled to room temperature and a sample of gaseous products for GC analysis was collected in a gas sampling bulb by controlled de-pressurization of the reactor. Weight of the liquid product after cooling and depressurization was noted so that mass fractions of liquid and gaseous products could be arrived at. Liquid and gaseous products were analysed by gas chromatography. Details on the analysis of product stream and computation of product stream composition are described in the Supplementary Data.

Results and Discussion

Characterization of catalysts

X-ray diffraction

Fig. 1 shows X-ray diffractograms of reduced catalysts. XRD for 8%Ni/5%CeO_2- Al_2O_3 (Fig. 1a) displays major d-lines due to gamma alumina phase, with the characteristic d-lines at 2θ values of 36.9°, 45.8° and 66.9° corresponding to (111), (400) and (440) planes, respectively, which are close to the reported 2θ values of 36.8°, 46.0° and 66.8° (JCPDS 46-1131). Besides, d-lines due to CeO_2 observed at 2θ values of 28.5° (111), 33.5° (211), 56.2° (311), 76.8° (420) are also in line with the reported 2θ values of 28.3º, 33.1°, 56.4° and 76.6° (JCPDS 34-0394). A weak line observed at 52.1° due to (200) plane in Ni metal is close to the reported value of 51.6º according to JCPDS-04-0850. The major d-line (111) due to Ni metal at 44.4° is very close to the broad d-line of alumina at 45.8º and hence not observed distinctly in Fig. 1a. However, expanded diffraction pattern in the 2θ range 43°-48° presented in Supplementary Data, Fig. S1a shows a weak line at 44.3° due to Ni metal. Similarly, in the case of 8%Co/5%CeO_2-Al_2O_3 catalyst (Fig. 1e) all major d-lines due to alumina and ceria phases are observed, besides the major d-line due to Co metal at 2θ-44.1° (44.3° as per JCPDS 15-0806) in Supplementary Data, Fig. S1e. In both cases, formation of Ni/Co aluminate with spinel structure is possible[32] but is not observed distinctly, since gamma alumina and the aluminates are iso-structural. In the diffractograms of other three Co-Ni mixed metal catalysts, all major d-lines due to alumina and

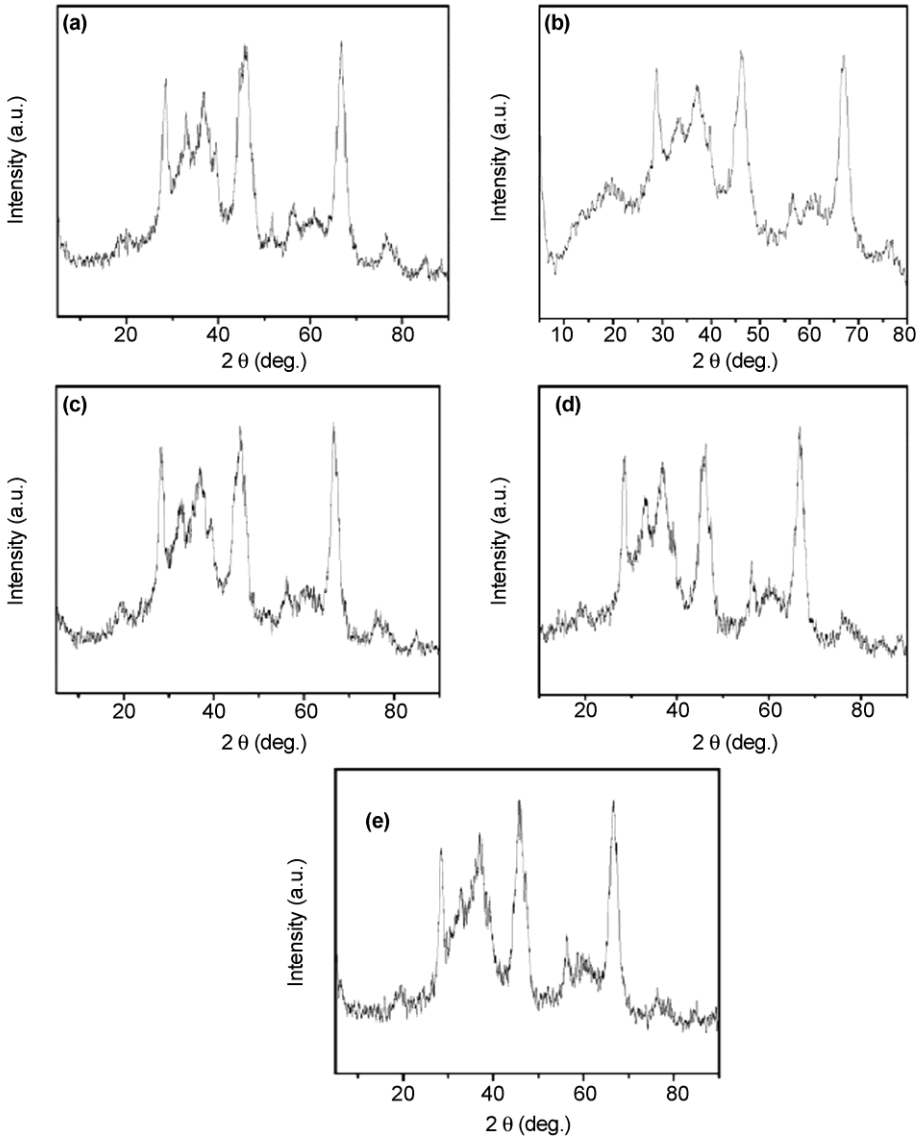

Fig. 1 — XRD pattern of the reduced catalysts: (a) 8%Ni/5%CeO_2-Al_2O_3, (b) 6%Ni-2%Co /5%CeO_2-Al_2O_3,(c) 4%Ni-4%Co/5%CeO_2-Al_2O_3, (d) 2.5%Ni-5.5%Co/5%CeO_2-Al_2O_3 and (e) 8%Co/5%CeO_2-Al_2O_3

ceria are displayed (Fig. 1b-d). XRD patterns in expanded mode corresponding to Fig. 1b-d as given in Supplementary Data, Fig. S1b to S1d, show weak d-lines at, 44.1°, 44.4° and 44.6°, respectively, shifted slightly from those due to Ni and Co metals, indicating possible formation of Ni-Co alloys[33]. Ni/Co crystallite size (8-10 nm) have been calculated using d-lines at 2θ= 52.1 to 52.5 corresponding to (200) planes, by applying Debye Scherrer equation (in Supplementary Data, Table S1).

Textural properties

The N_2 adsorption/desorption isotherms and pore size distribution profiles of reduced catalysts are shown in Supplementary Data, Fig. S2. The catalysts display Type-IV N_2 adsorption/desorption isotherms, and Type-H2 hysteresis loops, indicating mesoporous characteristics. As expected, no significant variations in the textural properties (surface area, pore volume and pore diameter) of ceria-alumina support, mono metallic Ni and Co and bimetallic Ni-Co catalysts are observed (in Supplementary Data, Table S1), since total metal loading is low, at 8% w/w.

Temperature programmed reduction (H_2-TPR)

H_2-TPR profiles for mono metallic Ni and Co, bimetallic Ni-Co catalysts, ceria modified alumina support are shown in Fig. 2. TPR profiles for the

catalysts, deconvoluted individually, for the analysis of reduction stages/reducible species are presented in Supplementary Data, Fig. S3 and a compilation of the reduction maxima observed accordingly for all the catalysts are presented in Table 1. Based on the literature data[34] on TPR studies on Ni/Al_2O_3 catalysts, three distinct reduction zones, in the temperature ranges 100-400 °C (Zone-1), 400-600 °C (Zone-2) and >600 °C (Zone-3), corresponding to the reduction of free and weakly bound NiO, well-dispersed NiO on alumina and Ni^{2+} in nickel aluminate lattice (due to strong metal- support interaction), respectively, are observed. Similar reduction zones are observed for supported cobalt catalysts as well. As shown in Fig. 2, ceria modified alumina support displays relatively very little reducibility (curve a) compared to the reducibility of Ni and Co. Hence reduction behaviours of only Ni and Co are discussed. Maximum H_2 consumption/ reducibility for all the catalysts is observed in the temperature range 400-600 °C (Zone-2) corresponding to the reduction of dispersed Ni and Co oxides. Maximum hydrogen consumption in Zone-2, amongst the catalysts, is observed for 8% Ni/CeO_2-Al_2O_3 (curve b). Introduction of 2% Co, brings down reducibility of dispersed Ni-Co oxides significantly (curve c). Catalyst with equal loading of Ni & Co (4% each), however, shows reducibility (curve d) higher than the formulations, 6% Ni-2%Co (curve c) and 2.5% Ni and 5.5% Co (curve e). Reducibility of catalyst with 8% Co loading (curve f) is again significantly lower vis-à-vis the catalyst with 8% Ni loading (curve c). Such variations in reducibility with respect to Ni-Co composition could play crucial role in ethanol conversion process. These details are discussed in the latter section.

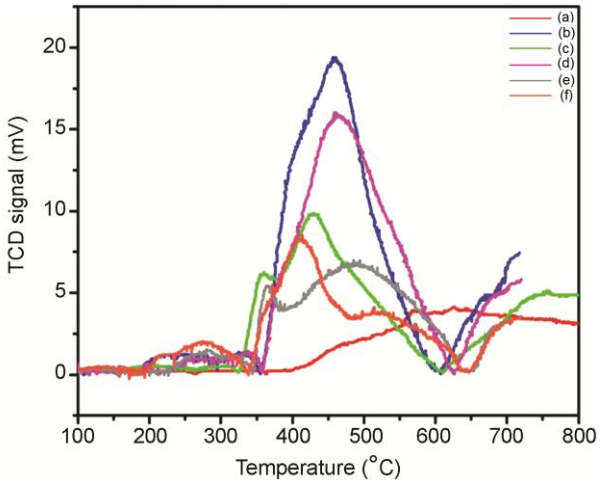

Fig. 2 — TPR profiles for Ni-Co/5% CeO_2 -Al_2O_3 catalysts: (a) 5%CeO_2-Al_2O_3, (b) 8%Ni/5%CeO_2-Al_2O_3, (c) 6%Ni-2%Co /5%CeO_2-Al_2O_3, (d) 4%Ni-4%Co/5%CeO_2-Al_2O_3, (e) 2.5%Ni-5.5%Co/5%CeO_2-Al_2O_3 and (f) 8%Co/5%CeO_2-Al_2O_3

TPR profiles after deconvolution bring out the presence of several reducible phases present in the catalysts. Seven reduction maxima indicating H_2 consumption are observed (in Supplementary Data, Fig. S3a) for the base catalyst, 8%Ni/5%CeO_2-Al_2O_3. Based on the literature data[34] on the reduction patterns for alumina supported Ni catalysts, the first two maxima at 239 °C, 325 °C, indicate the reduction of free and weakly bound NiO. Next three maxima at 403 °C, 459 °C and 507 °C are due to the reduction of well dispersed NiO species with weak interaction with the support. The maxima observed at 639 °C and 669 °C are attributed to the reduction of Ni^{2+} in nickel aluminate lattice.

Partial replacement of Ni towards the composition 2%Co-6%Ni/5%CeO_2-Al_2O_3 results in multiple reduction maxima due to the presence of reducible Ni and Co oxides in free or weakly bound state (211 °C, 300 °C, 360 °C), well-dispersed over the support (426 °C, 448 °C) and as Ni/Co aluminates due to strong interactions with the support (665 °C and 759 °C). Essentially, Ni and Co oxidic species undergo reduction separately, with little interaction between the species. When Co and Ni are present in equal proportions (4%Co-4%Ni/5%CeO_2-Al_2O_3), perceptible changes are observed in the reduction pattern. Reduction maxima at 360 °C, 426 °C and 448 °C for lower Co-content sample are shifted to

Table 1 — Temperature programmed reduction (TPR) characteristics of Ni-Co bimetallic catalysts

Catalysts	TPR maxima (°C)		
	Zone-I (100 °C – 400 °C)	Zone-II (400 °C – 600 °C)	Zone-III (600 °C – 800 °C)
8%Ni/5%CeO_2-Al_2O_3	239, 325	403, 459, 507	639, 669
6%Ni-2%Co/5%CeO_2-Al_2O_3	211, 300, 360	426, 488	665, 759
4%Ni-4%Co/5%CeO_2-Al_2O_3	266, 329, 391	473, 532	651, 686
2.5%Ni-5.5%Co/5%CeO_2-Al_2O_3	276, 312, 366	423, 489, 562	664, 690
8%Co/5%CeO_2-Al_2O_3	137, 235, 289, 375	409, 452, 514, 568	673

higher temperatures, 391 °C, 473 °C and 532 °C, indicating simultaneous reduction of Ni and Co oxide species, possibly leading to the formation of Ni-Co alloys. Significantly, the intensities of the low temperature reduction peaks at 266 °C and 329 °C, due to free oxides and high temperature peaks at 651 °C and 686 °C, for Ni^{2+}/Co^{2+} in the aluminate phases, are relatively lower, indicating that simultaneous reduction of Ni and Co oxidic species is the dominant process. Similar reports involving simultaneous reduction of Ni and Co oxidic species leading to the formation of Ni-Co alloys have been published earlier[32,35,36]. Reduction pattern observed for 5.5%Co-2.5%Ni/5%CeO_2-Al_2O_3 catalyst, also involves simultaneous reduction of Ni^{2+} and Co^{2+} involving alloy formation, along with reduction of dispersed Ni and Co oxides. The catalyst 8% Co/CeO_2-Al_2O_3 displays multiple reduction maxima due to the presence of different reducible phases of Co in +2 and +3 oxidation states. Reduction maxima in the range 200 °C-300 °C are due to weakly bound Co oxides. Different forms of oxidic cobalt in mixed valence states (+2 and +3) and dispersed with varying degree of interaction with the support, undergo reduction in the temperature range 300-600 °C, leading to multiple reduction maxima, while Co^{2+} in aluminate phase gets reduced at temperature >600 °C. Such non-uniform changes in the reducibility of Ni-Co system could be due to i) presence of different reducible species, like Ni^{2+}, Co^{2+} and Co^{3+} with varying degrees of dispersion and reducibility ii) variations in the degree of interaction of these species with the support (metal-support interactions)

X-ray photoelectron spectroscopy (XPS)

XPS profiles for the typical bi-metallic catalyst, 4%Co-4%Ni/5%CeO_2-Al_2O_3, are presented in Fig. 3. Binding energy (BE) values observed for Co $2p_{3/2}$ (779.1 eV) in Fig. 3a and Ni $2p_{3/2}$ (853.9 eV) in Fig.3b, are close to the values reported[37-40] for metallic Co (778.2 eV) and Ni (852.6 eV), thus confirming that in the catalyst, both Co and Ni are in metallic state. The shifts in BE values, with respect to those for clean metals, are due to the ceria modified alumina support effect and the electronic interactions between Co and Ni in metallic state, arising out of nanoscale alloy formation, as indicated in the TPR studies. Surface concentrations of Ni and Co computed from XPS data (Supplementary Data, Fig. S4) of the catalyst are nearly equal and the ratio is same as that in bulk composition, indicating that both metals are equally dispersed. XPS line observed at 860.8 eV (Fig. 3b) is attributed to Ni 2p for nickel aluminate phase[41]. The satellite peak observed at 784.6 eV (Fig. 3a) is due to the presence Co^{2+} in cobalt aluminate. XPS lines due to Ce^{4+} $3d_{3/2}$ core level are reported at 900.8 eV, 907.2 eV and 916.7 eV and $3d_{5/2}$ core levels at 882.4 eV, 888.8 eV and 898.1 eV.[42-45] Corresponding XPS lines for Ce^{3+} are expected at 903.7 eV, 884.7 eV, 899.2 eV and 880.1 eV[42,45,46]. In the present work, XPS lines (Fig. 3c) observed at 902.4 eV, 915.7 eV and 898.2 eV could be assigned to Ce^{4+} state and the lines at 880.3 eV, 884.2 eV and 899.2 eV to Ce $^{3+}$ state indicating the presence of Ce in mixed valence states.

Acidity and basicity of the catalysts

NH_3-TPD profiles for the catalysts in reduced state are given in Supplementary Data, Fig. S5 and the compilation of acidity and acid sites distribution are given in Table 2. All catalysts are characterized by the presence of weak (<250 °C), medium (300-400 °C) and strong (>400 °C) acid sites. No significant variations in the total acid sites distribution is observed when Ni and Co contents are varied, except for the higher value (0.8 mmol/g) for medium strength acid sites observed for 6%Ni-2%Co/5%CeO_2-Al_2O_3 catalyst, which could not be rationalized. However, in all catalysts, weak and medium strength acid sites are predominant over the strong acid sites. CO_2 TPD

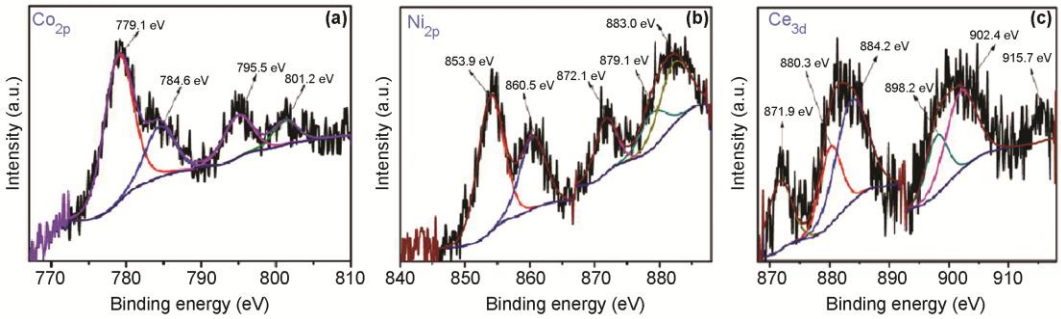

Fig. 3 — XPS spectra of the reduced catalyst - 4%Ni-4%Co/5%CeO_2-Al_2O_3: (a) Co_{2p}, (b) Ni_{2p} and (c) Ce_{3d}

Table 2 — Distribution of acid sites by ammonia TPD for bimetallic Ni-Co catalysts

Catalyst	Distribution of acid sites						
	Weak		Medium		Strong		Total acidity
	Temp. (°C)	Acidity (mmol/g)	Temp. (°C)	Acidity (mmol/g)	Temp. (°C)	Acidity (mmol/g)	(mmol/g)
8%Ni/5%CeO_2-Al_2O_3	187	0.299	366	0.316	447	0.151	0.766
6%Ni-2%Co/5%CeO_2-Al_2O_3	233	0.338	365	0.800	537	0.289	1.425
4%Ni-4%Co/5%CeO_2-Al_2O_3	199	0.382	365	0.220	462	0.121	0.723
2.5%Ni-5.5%Co/5%CeO_2-Al_2O_3	202	0.371	362	0.248	451	0.199	0.818
8%Co/5%CeO_2-Al_2O_3	213	0.399	339	0.242	446	0.167	0.808

Table 3 — Distribution of basic sites by CO_2 TPD for bimetallic Ni-Co catalysts

Catalyst	Distribution of Basic sites						
	Weak		Medium		Strong		Total basicity
	Temp. (°C)	Basicity (mmol/g)	Temp. (°C)	Basicity (mmol/g)	Temp. (°C)	Basicity (mmol/g)	(mmol/g)
8%Ni/5%CeO_2-Al_2O_3	209	0.037	361	0.207	529	0.049	0.293
6%Ni-2%Co/5%CeO_2-Al_2O_3	216	0.022	362	0.194	547	0.039	0.255
4%Ni-4%Co/5%CeO_2-Al_2O_3	119	0.007	359	0.232	527	0.045	0.284
2.5%Ni-5.5%Co/5%CeO_2-Al_2O_3	119	0.004	376/	0.216	598	0.042	0.284
8%Co/5%CeO_2-Al_2O_3	201	0.025	358/	0.133	511	0.055	0.213

profiles for the catalysts in reduces state are shown in Fig. S6 and Table 3 show total basicity and basic sites distribution data. Weak (<250 °C), medium (300-400 °C) and strong (>500 °C) basic sites are observed in all the catalysts. While very little variation in total basicity is observed along the series, basic sites of medium strength are predominant over weak and strong acid sites. The catalysts thus possess balanced acidic and basic sites required for condensation of ethanol to butanol and higher alcohols.

Diffuse reflectance spectroscopy

DRS of the catalysts in reduced state are presented in Fig. 4. In accordance with XRD and XPS data, some parts of Ni and Co are present as Ni^{2+} and Co^{2+} in aluminate phase. In the case of 8% Ni/CeO_2-Al_2O_3 absorption maximum observed at 320 nm is due to the presence of Ni^{2+} in octahedral co-ordination in nickel aluminate phase[47]. Presence of this maximum in all Ni-containing samples indicates that Ni^{2+} in the catalysts is present in octahedral sites. Introduction of Co in the place of Ni results in additional three distinct absorption maxima in the region 530-630 nm which are attributed to the presence of Co^{2+} in tetrahedral sites[48]. Absorption maxima due to Co^{2+} in octahedral sites, expected in the region 400-700 nm[48] are possibly merged with maxima due to Co^{2+} in tetrahedral sites. DRS studies thus reveal that Ni^{2+} ions in all the catalysts are present in octahedral sites while majority of Co^{2+} ions are present in tetrahedral sites.

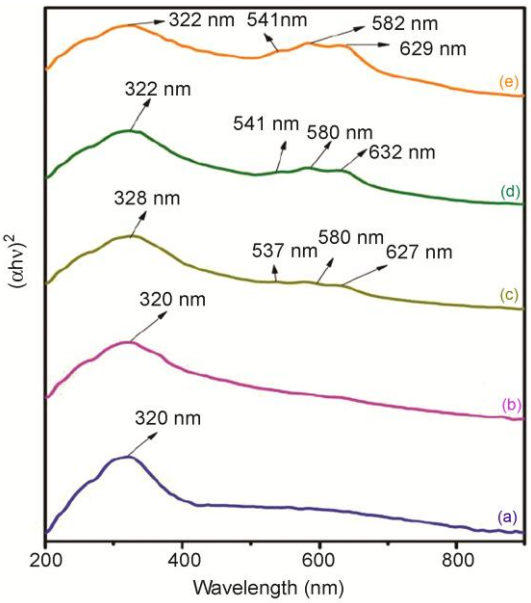

Fig. 4 — DRS-UV spectra of the reduced bimetallic Ni-Co catalysts: (a) 8%Ni/5%CeO_2-Al_2O_3, (b) 6%Ni-2%Co /5%CeO_2-Al_2O_3, (c) 4%Ni-4%Co/5%CeO_2-Al_2O_3, (d) 2.5%Ni-5.5%Co/5%CeO_2-Al_2O_3 and (e) 8%Co/5%CeO_2-Al_2O_3

Catalytic activity for condensation of ethanol

Distribution of products

Graphical representation of the data on the conversion of ethanol and selectivity to butanol and higher carbon number alcohols at 200 °C on Ni-Co series of bimetallic catalysts supported on ceria modified alumina is presented in Fig. 5 and the

respective values are compiled in Supplementary Data, Table S2 for easy reference. Detailed distribution of all compounds identified in the product streams for all the five catalysts are presented in Supplementary Data, Table S3. Butanol, hexanol and octanol are the major desired products and ethylene is the major by-product along with small amounts of C_1-C_5 hydrocarbons and oxides of carbon. Besides C_2-C_8 aldehydes, ketones and esters are observed in trace amounts. Overall product patterns for the five catalysts indicate that the process follows typical Guerbet chemistry pathway.

Ethanol conversion and selectivity trends

Ethanol conversion in the range 42% to 55% is realized on all catalysts, with bimetallic Ni-Co catalysts of specific compositions displaying higher selectivity towards butanol and higher alcohols vis-à-vis the corresponding mono metallic catalysts (Fig. 5 and in Supplementary Data, Table S2). There is a clear difference in ethanol conversion on 8% Ni/CeO_2-Al_2O_3 and 8% Co/CeO_2-Al_2O_3 with Co based catalyst displaying lower conversion (43.6% vs. 52.6% in Supplementary Data, Table S2), possibly due to the differences in the extent/strength of metal support interactions and consequently the reducibility. Monometallic Ni displays maximum reducibility (Fig. 2, profile-c) in the temperature range 400-600 °C (corresponding to reduction of dispersed metal oxides) compared to all bimetallic Ni-Co catalysts and mono metallic Co catalyst. According to Guerbet chemistry, presence of Ni and Co in metallic state is essential for dehydrogenation-hydrogenation reaction steps involved in the process for ethanol conversion to higher alcohols. TPR profiles indicate lower hydrogen consumption/reducibility for 8% Co catalyst vis-à-vis 8% Ni catalyst in the temperature range 400-600 °C due to stronger metal support interaction, (Fig. 2, profile c vs. profile g). On the same grounds, introduction of 2% Co brings down reducibility and hence conversion from 52.6 % to 42.2%. However, the catalyst with equal loading of Ni & Co displays high reducibility, due to simultaneous reduction of dispersed Ni^{2+} and Co^{2+}, involving alloy formation, resulting in higher conversion, 55% vs. 52.6% and higher selectivity for C_{4+} alcohols, 50.1% vs. 46.4%. Further increase in Co-content leads to slight decrease in conversion and so is the reducibility. Alloy formation is expected to play a crucial role, since both reducibility and activity/selectivity are high with 4%Ni-4%Co. Thus, the observed variations in conversion and selectivity could be explained on the basis of differences in the degree of metal support interactions, reducibility and consequently, the extent of alloy formation.

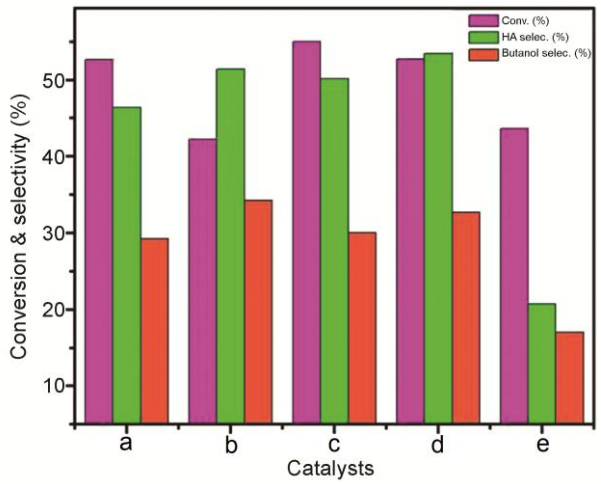

Fig. 5 — Ethanol conversion ( ), higher alcohol ( ) and butanol selectivity ( ) on catalysts at 200 °C: (a) 8%Ni/5%CeO_2-Al_2O_3, (b) 6%Ni-2%Co/5%CeO_2-Al_2O_3, (c) 4%Ni-4%Co/5%CeO_2-Al_2O_3, (d)2.5%Ni-5.5%Co/5%CeO_2-Al_2O_3 and (e) 8%Co/5%CeO_2-Al_2O_3

While monometallic Ni displays butanol selectivity of 29.2% and higher alcohol selectivity of 46.4%, corresponding values for monometallic Co-catalyst are lower, i.e. at 17% and 20.7%, respectively. These observations are in line with the earlier work reported for alumina supported Ni and Co catalysts[10,11a,11b]. Formation of ethyl acetate (in Supplementary Data, Table S3) is higher (5.23%) with monometallic Co and the catalyst with higher Co content, $Ni_{2.5}Co_{5.5}$/CeO_2-Al_2O_3 (1.06%) in comparison with that on monometallic Ni (0.69%), which is attributed to the presence of Co^{2+} in tetrahedral sites[11b]. DRS for Co containing catalysts (Fig. 4) reveal that majority of Co^{2+} ions in cobalt aluminate phase are in tetrahedral sites, while Ni^{2+} in nickel aluminate is in octahedral sites. Presence of Ni leads to substantial decrease in the formation of ethyl acetate and increase in butanol and higher alcohol selectivity with respect to mono metallic Co catalysts (in Supplementary Data, Table S3). While butanol selectivity remains nearly the same, higher alcohol selectivity increases possibly because butanol is consumed in the formation of higher alcohols. Hexanol, formed by aldol condensation of butanol and ethanol, is less on 8%Co catalyst since butanol formation itself is less. Significant amount of ethylene (12-17%) is formed on all the catalysts, by dehydration of diethyl ether, which in turn is formed from ethanol (Scheme 1), due

to inherent acidity of the catalysts. However, on mono metallic cobalt catalyst, ethane formation is relatively higher possibly via ethylene.

Role of Ni-Co alloys

Bimetallic Ni Co catalysts, especially with compositions 4%Ni-4%Co and 2.5%Ni-5.5%Co display higher ethanol conversion and higher alcohol selectivity with respect to mono metallic catalysts. XRD, H_2 TPR and XPS studies support the formation of nanoscale bi-metallic alloys of Ni and Co, which could play a pivotal role in this aspect. Formation of nanoscale alloys in supported Ni-Co bimetallic catalysts and its influence on the activity for reactions like, steam methane reforming [49], dry reforming of methane with CO_2[50, 51], steam reforming of alcohols[52] and acetic acid[53], hydrogenation of CO[54–56], methane partial oxidation[57], hydrogenation of furfural[58] and hydrogenation of benzaldehyde[59] have been documented in literature. Ni–Co alloys are known to generate active hydrogen, which suppress coke formation and retard deactivation, possibly by hydrogenation of coke precursors. Ni-Co alloy formation in titania supported catalysts and generation of active hydrogen, as indicated by H_2 TPD studies [60], leads to higher activity for hydrogenation of cinnamaldehyde vis-à-vis mono metallic catalysts.

In the present work, ethanol conversion on ceria-alumina supported Ni-Co catalysts follows Guerbet chemistry pathway, wherein, dehydrogenation of ethanol to acetaldehyde, followed by aldol condensation to crotonaldehyde, butyraldehyde and higher carbon number aldehydes and their subsequent hydrogenation to butanol and higher alcohols, are the crucial steps. (Scheme 1). Acidity and basicity (for aldol condensation) and dehydrogenation-hydrogenation (for ethanol dehydrogenation to acetaldehyde and hydrogenation of C_4 and higher carbon number aldehydes) are the essential catalytic functionalities.

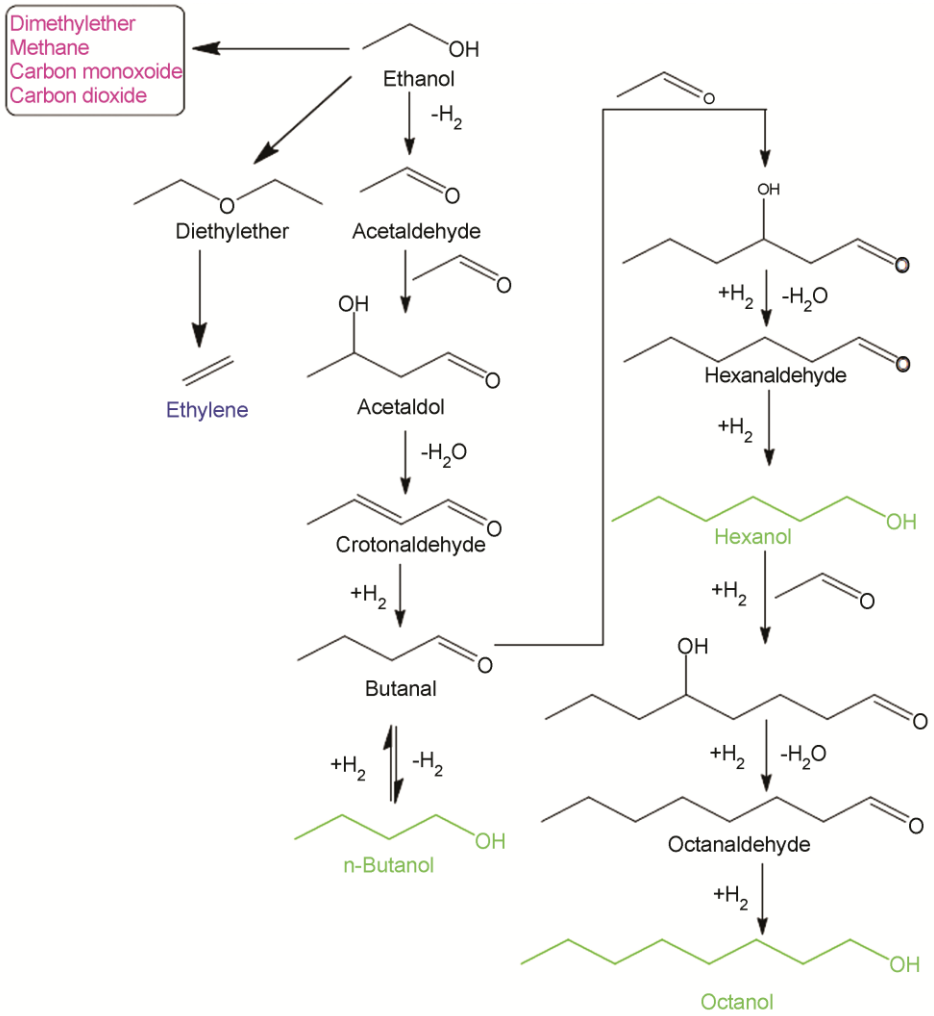

Scheme 1 — Reaction for conversion of Ethanol to Butanol

While acidity-basicity originates from the support and Ni/Co aluminate phases, dehydrogenation-hydrogenation originates from the metal sites. Role of metal sites is thus crucial, since they are involved in the initial dehydrogenation and final hydrogenation steps. Compared to the monometallic (Ni/Co) catalysts, bimetallic Ni-Co catalysts are known to exhibit higher activity due to the synergetic interactions and alloy formation. In this context, formation of Co-Ni nanoscale alloys in Ni-Co bimetallic catalysts with higher activity for dehydrogenation and hydrogenation reactions are responsible for the observed higher activity and selectivity for butanol and higher alcohols. Thus, the choice of bimetallic catalysts with specific composition range seems to be a good strategy for achieving higher ethanol conversion and selectivity for higher alcohols.

Sun et al.[13] have reported ethanol conversion of 56% and butanol yield of 22% on bimetallic Ni-Cu catalysts supported on Mg-Al-O mixed oxides, but at higher temperature of 320 °C. Au based bimetallic catalysts, Au-Ni and Au-M, with M= Fe, Co, Ag and Zr, studied by Chistyakov et al., and Nikolev et al.[16] respectively, display good activity and higher alcohol selectivity, again at higher temperature, at 275 °C, under super critical conditions. Another recent publication[31] on the application of tri-metallic Cu-Ni-Mn catalysts for ethanol conversion reports lower activity and selectivity. In comparison, the Ni-Co bimetallic catalysts reported in the present work display better activity and selectivity at lower temperature of 200 °C.

Conclusions

A new series of Ni-Co bimetallic catalysts with varying nickel and cobalt contents and supported on CeO_2(5% w/w)-Al_2O_3 mixed oxide has been prepared and evaluated for activity for condensation of ethanol and selectivity for butanol and higher alcohols. XRD, TPR and XPS studies reveal the formation of nickel-cobalt alloys, especially with compositions, 4%Ni-4%Co and 2.5%Ni-5.5%Co. Higher ethanol conversion and selectivity for higher alcohols are observed with the same catalyst compositions. Dehydrogenation of ethanol to acetaldehyde and hydrogenation of C_4 and higher aldehydes are the key steps in ethanol condensation process. Ni-Co alloys promote both dehydrogenation and hydrogenation steps, thus leading to improvements in ethanol conversion and selectivity for higher alcohols.

Supplementary Data

Supplementary Data associated with this article are available in the electronic form at http://nopr.niscair.res.in/jinfo/ijca/IJCA_60A(03)386-396_SupplData.pdf.

Acknowledgement

The authors are grateful to DST, GOI, New Delhi, for providing the research facilities at NCCR, IIT Madras, Chennai and adequate instrumentation facilities for characterization of catalysts in the Department of Chemistry, Anna University, Chennai.

References

1 Tsuchida T, Sakuma S, Takeguchi T & Ueda W, *Ind Eng Chem Res*, 45 (2006) 8634.
2 Breitkreuz K, Menne A & Kraft A, *Biofuels Bioprod Biorefin*, 8 (2014) 504.
3 Renewable Fuels Association. http://www.ethanolrfa.org/resources/industry/statistics/#1454098996479-8715d404-e546 - Accessed on 19th June 2019.
4 Angelici C, Weckhuysen B M & Bruijnincx P C A, *ChemSusChem*, 6 (2013) 1595.
5 (a) Guerbet M, *C R Acad Sci Paris*, 128 (1899) 1002; (b) Guerbet M, *C R Acad Sci Paris*, 149 (1909) 129.
6 Wu X, Fang G, Tong Y, Jiang D, Liang Z, Leng W, Liu L, Tu P, Wang H, Ni J & Li X, *ChemSusChem*, 11 (2018) 71.
7 Aitchison H, Wingad R L & Wass D F, *ACS Catal*, 6 (2016) 7125.
8 (a) Kozlowski J T & Davis R J, *ACS Catal*, 3 (2013) 1588; (b) Galadima A & Muraza O, *Ind Eng Chem Res*, 54 (2015) 7181.
9 Cimino S, Lisi L & Romanucci S, *Catal Today*, 304 (2018) 58.
10 Ke Wu Yang X, Jiang Z & Zhang W C, *Chin Chem Lett*, 15 (2004) 1497.
11 (a) Riittonen T, Toukoniitty E, Madnani D K, Leino A R, Kordas K, Szabo M, Sapi A, Arve K, Wärna J & Mikkola J P, *Catalysts*, 2 (2012) 68; (b) Riittonen T, Ernen K, Mäki-Arvela P, Shchukarev A, Rautio A R, Kordas K, Kumar N, Salmi T & Mikkola J P, *Renew Energy*, 74 (2015) 369.
12 Jordison T L, Lira C T & Miller D J, *Ind Eng Chem Res*, 54 (2015) 10991.
13 Sun Z, Vasconcelos A C, Bottari G, Stuart M C A, Bonura G, Cannilla C, Frusteri F & Barta K, *ACS Sustain Chem Eng*, 5 (2017) 1738.
14 Ghaziaskar H S & Xu C (Charles), *RSC Adv*, 3 (2013) 4271.
15 Pang J, Zheng M, He L, Li L, Pan X, Wang A, Wang X & Zhang T, *J Catal*, 344 (2016) 184.
16 (a) Chistyakov A V, Zharova P A, Nikolaev S A & Tsodikov M V, *Catal Today*, 279 (2017) 124; (b) Chistyakov A V, Zharova P A, Tsodikova M V, Nikolaev S A, Krotova I N & Ezzhelenko D I, *Kinet Catal*, 57 (2016) 803; (c) Nikolaev S A, Tsodikov M V, Chistyakov A V, Zharova P A & Ezzgelenko D I, *J Catal*, 369 (2019) 501.
17 Quesada J, Arreola-Sánchez R, Faba L, Díaz E, Rentería-Tapia V M & Ordóñez S, *Appl Catal A*, 551 (2018) 23.
18 Ni Li X, Peng S S, Feng L N, Lu S Q, Ma L J & Yue M B, *Micropor Mesopor Mat*, 261 (2018) 44.
19 Zaccheria F, Scotti N & Ravasio N, *Chem Cat Chem*, 10 (2018) 1.

20 Quesada J, Faba L, Díaz E & Ordóñez S, *Appl Catal A*, 559 (2018) 167.
21 Earley J H, Bourne R A, Watson M J & Poliakoff M, *Green Chem*, 17 (2015) 3018.
22 Perronea O M, Lobefaro F, Aresta M, Nocito F, Boscolo M & Dibenedetto A, *Fuel Process Technol*, 177 (2018) 353.
23 Apuzzo J, Cimino S & Lisi L, *RSC Adv*, 8 (2018) 25846.
24 Vinayagamoorthi R, Shanthi K, Thirunavukkarasu K, Krishnamurthy K R & Viswanathan B, *Indian J Chem Technol*, (Accepted).
25 Zhang X, Liu Z, Xu X, Yue H, Tian Ge & Feng S, *ACS Sustain Chem Eng*, 1 (2013) 1493.
26 Quesada J, Faba L, Díaz E & Ordóñez S, *Appl catal A*, 542 (2017) 271.
27 Quesada J, Faba L, Díaz E & Ordóñez S, *Appl catal A*, 559 (2018) 167.
28 Quesada J, Faba L, Díaz E & Ordóñez S, *Appl catal A*, 563 (2018) 64.
29 Xiao Z, Li L, Wu C, Li G, Liu G & Wang L, *Catal Lett*, 146 (2016) 1780.
30 Wu X, Fang G, Liang Z, Leng W, Xu K, Jiang D, Ni J & Li X, *Catal Commun*, 100 (2017) 15.
31 Lopez-Olmos C, Guerrero-Ruiz A & Rodríguez-Ramos I, *Catal Today*, 351 (2020) 132
32 Yang R, Li X, Wu J, Zhang X & Zhang Z, *J Phys Chem C*, 113 (2009) 17787.
33 (a) Xiao Z, Li L, Wu C, Li G, Liu G & Wang L, *Catal Lett*, 146 (2016) 1780; (b) Xu J, Zhou W, Li Z, Wang J & Ma J, *Int J Hydrog Energy*, 34 (2009) 6646.
34 (a) Tribalis A, Panagiotou G D, Bourikas K, Sygellou L, Kennou S, Ladas S, Lycourghiotis A & Kordulis C, *Catalysts*, 6 (2016) 11; (b) Sánchez- Sánchez M C & Navarro R M, *Int J Hydrog Energy*, 32 (2007) 1462; (c) Ponminiessarry R P, Ph.D Thesis, Cochin University of Science and Technology, Cochin, (2010).
35 Xu J, Zhou W, Li Z, Wang J & Ma J, *Int J Hydrog Energy*, 34 (2009) 6646.
36 Zhang J G, Wang H & Dalai A K, *J Catal*, 249 (2007) 300.
37 Takanabe K, Nagaoka K, Nariai K & Aika K, *J Catal*, 232 (2005) 268.
38 McIntyre N S & Cook M G, *Anal Chem*, 47 (1975) 2208.
39 Skriver H L & Rosengaard N M, *Phys Rev B*, 46 (1992) 7157.
40 Grosvenor A P, Biesinger M C, Smart R St C & McIntyre N S, *Surf Sci*, 600 (2006) 1771.
41 (a) Bunch A Y, Wang X Q & Ozkan U S, *J Mol Catal A*, 270 (2007) 264; (b) Ding L H, Zheng Y, Zhang Z S, Ring Z & Chen J W, *J Catal*, 241 (2006) 435.
42 Nelson A E & Schulz K H, *Appl Surf Sci*, 210 (2003) 206.
43 Jiang L, Zhu H, Razzaq R, Zhu M, Li C & Li Z, *Int J Hydrog Energy*, 37 (2012) 15914.
44 Murugan B, Ramaswamy A V, Srinivas D, Gopinathand C S & Ramaswamy V, *Chem Mater,* 17 (2005) 3983.
45 Pfau A & Schierbaum K D, *Surf Sci*, 321 (1994) 71.
46 Zhang F, Wang P, Koberstein J, Khalid S & Chan S W, *Surf Sci*, 563 (2004) 74.
47 Scheffer B, Heijeinga J J & Moulijn J A, *J Phys Chem*, 91 (1987) 4752.
48 (a) Ram´ırez J, Contreras R, Castillo P, Klimova T, Zárate R & Luna R, *Appl Catal A*, 197 (2000) 69; (b) Gajardo P, Grange P & Delmon B, *J Catal*, 63 (1980) 201.
49 You X, Wang X, Ma Y, Liu J, Liu W, Xu X, Peng H, Li C, Zhou W, Yuan P & Chen X, *Chem Cat Chem*, 6 (2014) 3377.
50 Takanabe K, Nagaoka K, Nariai K & Aika K, *J Catal*, 232 (2005) 268.
51 Phongaksorn M, Tungkamani S, Dharmasaroja N, Chamni T, Chuvareec R, Kanjanabat N & Siri-Nguanc N, *Chem Eng Trans*, 43 (2015) 925.
52 Hu X & Lu G X, *J Mol Catal A*, 261 (2007) 43.
53 Chen L W, Choong C K S, Zhong Z Y, Huang L, Wang Z & Lin J Y, *Int J Hydrog Energy*, 37 (2012) 16321.
54 Woo H, Srinivasan R, Rice L, De Angelis R & Reucroft P, *J Mol Catal*, 59 (1990) 83.
55 Tatsumi I, Koichi E & Hiromichi A, *Appl Catal*, 30 (1987) 225.
56 Das P C, Pradhan N C, Dalai A K & Bakshi N N, *Catal Lett*, 98 (2004) 153.
57 Luo H, Li H & Zhuang H L, *Chem Lett*, 5 (2001) 404.
58 Wei L, Xianian C, Jin L, Ying Y, Yongfu Z, Zhaolong H & Zhengzhou Y, *Adv Mat Res*, 430 (2012) 917.
59 Lin W, Chang H, He L, Yu Y & Zhang F, *J Catal*, 303 (2013) 110.
60 Saranya A, Ganesan V, Krishnamurthy K R & Viswanathan B, *Res Chem Intermed*, 44 (2018) 6703.